Transport properties of 3D extended s-wave states in Fe-based superconductors

V. Mishra[1], S. Graser[2] and P. J. Hirschfeld[1]

[1] *Department of Physics, University of Florida, Gainesville, FL 32611, USA*
[2] *Center for Electronic Correlations and Magnetism, Institute of Physics,*
University of Augsburg, D-86135 Augsburg, Germany
(Dated: August 2, 2011)

The Fermi surfaces of Fe-pnictide superconductors are fairly two-dimensional (2D), and it has thus come as a surprise that recent penetration depth and thermal conductivity measurements on systems of the 122 type have reported c-axis transport coefficients at low temperatures in the superconducting state comparable to or even larger than that in the ab-plane. These results should provide important information on both the Fermi surface and the superconducting state. Here we consider the theory of the superfluid density and thermal conductivity in models of extended-s wave superconducting states expected to be appropriate for Fe-pnictide systems. We include intraband disorder and consider a range of different Fermi surfaces where gap nodes might exist. We show that recent experiments on $Ba(Fe_{1-x}Co_x)_2As_2$ can be semiquantitatively understood by such an approach, and discuss their implications.

PACS numbers:

I. INTRODUCTION

The new Fe-based superconductors have captured the imagination of the theoretical and experimental superconductivity community, in part because the critical temperature T_c is high in certain materials, but also because the phenomenology of the superconducting state appears to be quite different from any class of novel superconductors heretofore discovered[1,2]. Since calculations of the coupling strength λ_{el-ph} due to the electron-phonon interaction show it to be small[3–5], it is believed that electronic pairing is predominant; thus attention has focussed on sign-changing states with A_{1g} symmetry predicted by spin fluctuation theory[6–12]. Depending on the details of the microscopic pair interaction[9,13,14] such states may display "accidental" nodal structures, nodes not dictated by symmetry considerations. It is important to understand such structures, as they provide clues to the origin of pairing.

In the LaFePO, KFe$_2$As$_2$, and BaFe$_2$(As$_{1-x}$P$_x$)$_2$ systems there is considerable evidence for low-energy excitations which could be produced by order parameters with nodes, but the structure of the nodal manifold is still controversial. In the heavily-studied $Ba(Fe_{1-x}Co_x)_2As_2$, $Ba(Fe_{1-x}Ni_x)_2As_2$ and BaFe$_2$(As$_{1-x}$K$_x$)$_2$ systems, which we will refer to collectively as Ba-122, measurements have been interpreted variously in terms of fully gapped behavior, deep minima in the superconducting gap, or gap nodes, and there is some evidence that these conclusions may be quite doping-dependent. The experimental probe which has thus far provided the lowest temperature information on the bulk order parameter is thermal conductivity. In the 122 systems, the ab-plane thermal conductivity data exhibited zero or extremely small linear-T term in zero magnetic field, reflecting the apparent absence of any nodes in the superconducting gap. The field dependence, however, was significantly stronger than that expected

for a large-gap superconductor[15–17]. This was analyzed by Mishra *et al.*[18] in terms of a gap with A_{1g} symmetry with no nodes but deep minima on the electron sheets. Bang proposed that this effect could also be explained phenomenologically by an isotropic A_{1g} state with very small gap on one Fermi surface sheet[19].

Recently, Martin *et al.*[20] reported a strong linear-T behavior of the magnetic penetration depth for currents along the c-axis in overdoped $Ba(Fe_{1-x}Ni_x)_2As_2$ crystals, compared to a predominantly T^2 behavior in the ab-plane, with possible much smaller ab linear-T contributions for some dopings. These authors pointed to a need for theoretical analysis of superconductivity in these materials beyond 2D models. Subsequently Reid *et al.*[21] measured a significant linear-T term in the low-T c-axis thermal conductivity of $Ba(Fe_{1-x}Co_x)_2As_2$ crystals, compared to a smaller or zero linear term in the ab-plane. In addition, the anisotropy ratio $(\kappa_c/\kappa_{c,N})/(\kappa_a/\kappa_{a,N})$ of the electronic thermal conductivities normalized to their values at T_c determined via resistivity measurements and the Wiedemann-Franz law, was found to increase rapidly as the crystal was doped away from optimal T_c. These authors argued that such an anisotropy ratio could arise only from gap nodes located precisely at flared regions of the quasi-cylindrical Fermi surfaces where $v_{F,c}/v_{F,a} \gg 1$, such that the corresponding κ_a arising at low T from the nodal structures would be negligible.

For some samples, Reid *et al.* reported a nonzero limiting value of $\kappa_{ab}(T)/T$ of order 1 μW/K^{2}cm. It is important to note that these values are much smaller than the value predicted in the simple BCS theory of quasiparticle transport in a nodal superconductor, of order $\kappa/T \approx N_0 v_F^2/(k_F v_\Delta)$, where N_0 is the Fermi level density of states and v_F is the Fermi velocity and v_Δ is the gap velocity $v_\Delta \equiv \partial\Delta_{\mathbf{k}}/\partial\mathbf{k}|_{\text{node}}$. This value is also much smaller than that observed in the cuprate case[22]. The low-T linear term in the thermal conductivity is expected to be universal (disorder-independent for weak disorder)

in the p-wave or d-wave case[23,24]. Mishra *et al.*[18] showed recently that this expression continues to hold in the extended-s type states thought to be characteristic of Fe-pnictide systems, but that universality breaks down effectively due to the strong dependence of v_Δ on disorder.

Theory has also made some recent progress in dealing with deviations from pure 2D behavior. Early spin fluctuation calculations for the pairing state of the Fe-pnictide materials[6,7,10,25] found that, depending on details of electronic structure and interaction parameters, nodes could occur on the electron sheets, but the gap on the hole sheets was always fairly large and isotropic. On the other hand, Graser *et al.*[26] recently presented a calculation of spin-fluctuation pairing in the 122 systems based on an RPA treatment of a 5-orbital model derived from density functional theory (DFT) electronic structure. In some cases, particularly for substantial hole doping, the ground state was found to be of A_{1g} symmetry, as in the 2D case, but while the electron sheet gap was found to be highly anisotropic but nodeless, the hole sheet was found to have nodes near the top of the Brillouin zone near the point where the Fermi surface sheets experience some outward flaring. Similar results were subsequently obtained by Kuroki *et al.* for $BaFe_2(As_{1-x}P_x)_2$[27].

In this work, we consider various possible Fermi surface geometries and gap structures which may give rise to the unusual low transport anisotropy seen in Refs. 21,28, bearing in mind that any phenomenology which purports to explain the results of these works must also be consistent with the earlier thermal conductivity results of Refs. 15–17. Although we consider 3D order parameter structures of the type found in Graser *et al.*[26], we do not attempt to tie our calculations or parameters to any particular microscopic calculation of either the Fermi surface or gap function, but rather to place restrictions on what types of structures are possible on the basis of these measurements. We argue that gap structures with small nodal segments near the $k_z = \pm\pi$ sections of flared Fermi surfaces are the most likely way to explain the unusual anisotropy in κ/T, the small size of these linear terms, and the magnetic field dependence observed. To some extent our calculations also depend on the role of disorder in these materials, which is not completely understood. In Section II, we present the model we study, in Section III give our results, in Section IV discuss them in comparison with experiment, and in Section V, conclude and critically consider the limitations of our approach.

II. MODEL

A. Fermi surfaces and gap structures

The purpose of this study is to examine transport in the superconducting state at very low energies; to this end, only the structure of the Bogliubov quasiparticle spectrum near gap nodes or deep minima is relevant.

In theoretical studies of these systems performed thus far, nodal structures in A_{1g} states have been obtained on either electron or hole pockets, but not both. We therefore consider two Fermi surface sheets, one of which (S_1) possesses gap nodes. The second (S_2) will be assumed to have deep gap minima, or to be irrelevant altogether for extremely low-energy transport. Results are symmetrized to ensure invariance under point group rotations. For the 122 systems, we will have in mind primarily that sheet S_1 is one of the hole sheets[26] and that S_2 is the (properly symmetrized) electron sheet. The reason is that, to the extent that nodes are occasionally found in spin fluctuation calculations on the electron sheets, they tend to run vertically from bottom to top of the Brillouin zone, and would therefore lead to an extremely large thermal conductivity anisotropy κ_{ab}/κ_c, in apparent contradiction to experiment. However, none of the results actually depend on the assignment of S_1 and S_2.

Fig. 1 shows various different kinds of Fermi surfaces S_1 and nodal structures which we consider in this work. Among the figures labeled "S_1", example 1 is a Fermi surface fit to the hole-doped α_1 sheet of Ref. 26, calculated using a 5-orbital fit to a first principles calculation for $BaFe_2As_2$ using the Quantum ESPRESSO package, assuming fixed experimentally determined atomic positions in the unit cell. The nodal line structures considered here are typical of the 3D ground states found on the α_1 and α_2 sheets in that work. Example 2 is the same Fermi surface with horizontal nodes found in the same case in Ref. 26 on the α_1 sheet. Example 3 is a model Fermi surface with identical topology but increased flaring near the top and bottom zone faces, with assumed V-shaped nodes near the flared portion. This Fermi surface is obtained within the same calculational scheme[26] for the α_2 Fermi surface, but using a structural optimization of the internal coordinate of the As position. In both calculations we have used $a = 3.9625$ Å and $c = 13.0168$ Å. Similar results are found elsewhere[29–31]. ARPES has provided some evidence for flaring of hole Fermi surfaces with large $v_{F,c}$ near the zone top[32–35], increasing with Co concentration, but at this writing there is no complete consensus on the 3D Fermi surface of the doped materials. Example 4 is the same Fermi surface but with horizontal nodes close to the k_z value where $v_{F,c}$ takes on a maximum. Example 5 is a model surface similar to that found in density functional theory calculations upon electron doping of the α_1 sheet together with a model gap structure giving nodes on the top surface. Finally, the last panel in Fig. 1 shows the second sheet S_2, fit to the Quantum ESPRESSO calculation for the electron sheets of $BaFe_2As_2$ for unrelaxed As coordinate, which is assumed to exist together with each of the cases 1-5 for S_1. We emphasize that our point of view here is that of phenomenologists; we allow ourselves to ask what would be the consequences if the Fermi surfaces actually took the forms shown for any of the doped materials.

A crucial ingredient in the calculations presented below are the Fermi velocities near the nodal surfaces. In Table

TABLE I: The DFT root mean square (rms) values of the in-plane and the out-of-plane component of the Fermi velocity on the different hole pockets S_1 and on the electron pocket S_2. In addition the rms values of the Fermi velocity components on the hole pockets, averaged only over the nodal regions, are tabulated. All values have been renormalized downward by a factor of 4 to account many-body effects and, are given in units of $10^5 \frac{m}{s}$. In the last lines are listed the r_z parameters in Eqs. 1-2 which determine the order parameter on the S_1 Fermi surfaces used to calculate results in this work, and the gap magnitude parameter Δ_0(meV).

	$S_1(1)$	$S_1(2)$	$S_1(3)$	$S_1(4)$	$S_1(5)$	S_2
$v_{F\perp}$	1.977	1.977	1.826	1.826	1.74	3.021
$v_{F,z}$	0.293	0.293	1.277	1.277	0.683	0.562
$v_{F\perp}^{node}$	2.074	2.037	2.076	1.546	1.067	
$v_{F,z}^{node}$	0.473	0.433	1.197	2.591	0.792	
r_z	0.9	-1.4	0.9	1.2	1.1	0.9
Δ_0	-8.6	9.1	-8.6	-9.4	-8.4	1.5

I, we list some values of Fermi velocity components and certain averages which will be important in the discussion below for the various cases for sheet S_1 and our fixed choice of S_2. The k_z dependence of the Fermi velocity components is exhibited in Figure 1.

In calculations of observables presented below, we have *reduced* all Fermi velocities shown in Table 1 by a factor of 4 to account for the effective renormalization of the bands with respect to DFT seen in ARPES which appears to be between 1.5 and 6 for all Fe-based superconducting materials[33,36]. There may be an additional low-energy renormalization at the meV scale, as discussed by Benfatto *et al.*[37]. All of these many body effects are lumped into a single doping– and momentum–independent renormalization of the Fermi velocity here, to get the crudest description of the anisotropy of transport properties driven by the underlying anisotropy of the DFT Fermi surface.

The model we adopt for the order parameter is a 3D extension of the phenomenological form treated, e.g. in Ref. 18. To obtain strictly horizontal nodes (cases 2,4,5), we consider gaps of the form

$$\Delta(k_z) = \Delta_0[1 + r_z \cos(k_z d)], \qquad (1)$$

whereas V-shaped nodal structures (cases 1,3) similar to that found in Ref. 26 (see Fig. 1) are produced by

$$\Delta(k_z, \phi) = \Delta_0[1 + r_z \cos(4\phi)(1 - \cos(k_z d))], \quad (2)$$

with $r_z > 1$ for the first kind of order parameter and $r_z > 0.5$ for the second kind of order parameter. In Fig. 1 for simplicity we have shown only the nodal surfaces of the order parameters chosen on the various Fermi surfaces, together with the variation of the Fermi velocity on those surfaces as a function of k_z.
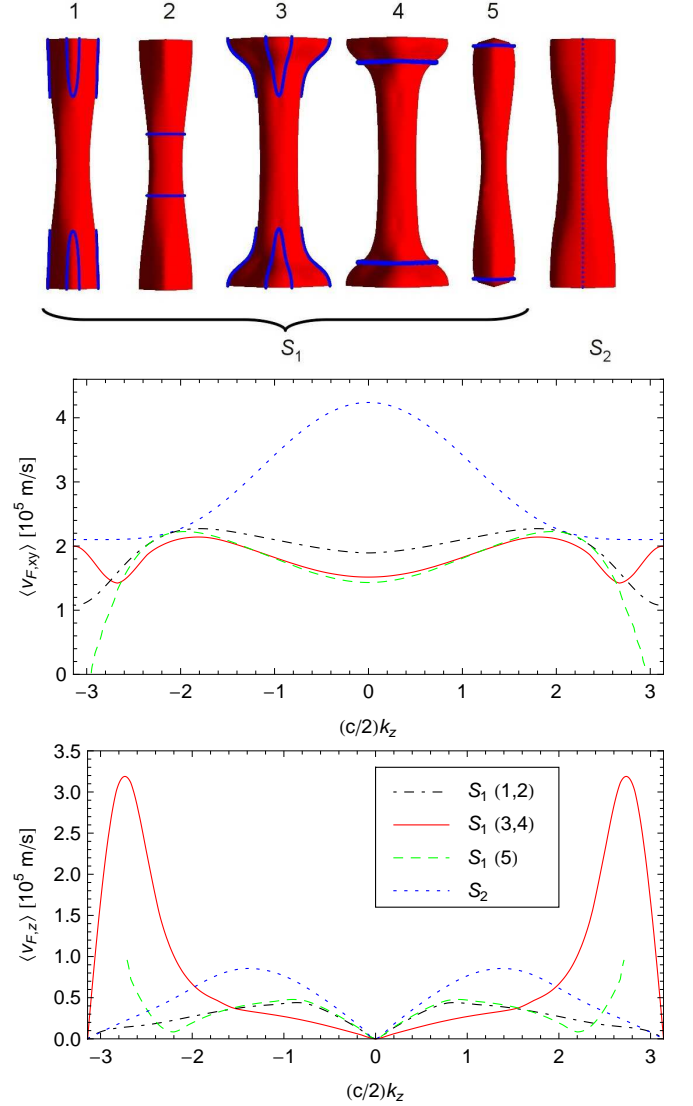

FIG. 1: Top: various different Fermi surfaces S_1 cases 1-5 and associated gap nodal structures (dark blue lines) considered in this work. Top right: sheet S_2 considered for all cases, with lines of deep gap minima (dark blue dashed lines) indicated. Bottom: Fermi velocity components $v_{F,xy} \equiv \sqrt{v_{F,x}^2 + v_{F,y}^2}$ and $v_{F,z}$ plotted vs. k_z for the five S_1 cases. Fermi velocities used in calculations are a constant factor of 2 smaller than those shown here. See text for discussion.

B. Disorder in 2-sheet pairing model

For disorder, we will assume an orbital-independent matrix element which scatters quasiparticles either within a given band with amplitude U_{ii}, $i = 1, 2$, or between bands with amplitude U_{12}. We sum all single-site scattering processes of arbitrary strength to obtain a disorder-averaged Nambu self energy $\underline{\Sigma} = n_{imp}\underline{T}$, where n_{imp} is the concentration of impurities, and $\underline{T}$ is the impurity T-matrix as parameterized e.g. in Ref. 18. For simplicity, we assume $U_{11} = U_{22} \equiv U_d$, with equal den-

sities of states $N_i = N_0$ throughout the paper. In our preliminary considerations we restrict ourselves to purely intraband scattering, $U_{12} = 0$. The disorder is characterized by two intraband scattering parameters on each sheet: $\Gamma_i \equiv n_{imp}/(\pi N_i)$ and $c_i = 1/(\pi N_i U_{ii})$; For our simple initial case with 2 symmetric bands we set $\Gamma_i = \Gamma$ and $c_i = c$, $i = 1, 2$. We only consider intraband scattering in the unitary limit[38], and further note that nonzero interband scattering does not affect the physics qualitatively, unless the interband scattering is as strong as the intraband scattering[39]. In presence of such strong isotropic scattering, one would expect a large suppression of T_c which is not observed in experiments.

The disorder-averaged matrix Green's function in the presence of scattering in the superconducting state is given by a diagonal matrix in band space,

$$\underline{G}(\mathbf{k}, \omega) = \frac{\tilde{\omega}\tau_0 + \tilde{\epsilon}_\mathbf{k}\tau_3 + \tilde{\Delta}_\mathbf{k}\tau_1}{\tilde{\omega}^2 - \tilde{\epsilon}_\mathbf{k}^2 - \tilde{\Delta}_\mathbf{k}^2}, \tag{3}$$

where $\mathbf{k} = \mathbf{k}_i \in S_i$ is restricted to Fermi surface sheet S_i with $i = 1, 2$, and the renormalized quantities $\tilde{\omega} \equiv \omega - \Sigma_0$, $\tilde{\epsilon}_\mathbf{k} \equiv \epsilon_\mathbf{k} + \Sigma_3$, $\tilde{\Delta}_\mathbf{k} \equiv \Delta_\mathbf{k} + \Sigma_1$ also depend on the band indices through $\mathbf{k}$. The Σ_α are the components of the self-energy proportional to the Pauli matrices τ_α in particle-hole (Nambu) space.

III. RESULTS

A. DOS

Below we focus on several bulk observables. It is useful to start with the analysis of the total density of quasiparticle states (DOS)

$$N(\omega) = -\frac{1}{2\pi}\text{Tr Im}\sum_{\mathbf{k}_i} \underline{G}(\mathbf{k}_i, \omega), \tag{4}$$

where the momentum summation indicates the explicit integration over distinct Fermi surface sheets with momenta $\mathbf{k}_i$. The total residual density of states (DOS) at the Fermi level $N(0)$ contains vital information about the low lying quasiparticle excitations and will determine all leading low temperature power laws. This quantity is sensitive to disorder or magnetic field. To give the reader a sense of the average density of quasiparticle excitations without reference to Fermi surface anisotropy, we calculate the residual DOS as a function of normal state scattering rate due to intraband disorder. Figure 2 shows $N(0)$ for the five different cases in consideration; generally it first increases with disorder, attains a maximum value and rapidly drops to zero again. This "reentrant" gapped behavior is a consequence of the node lifting phenomena characteristic of accidental nodes in an order parameter with A_{1g} symmetry[18,40]. Considering the evidence provided by Refs. 20,21 for low-energy excitations, we assume in our discussion below that we are
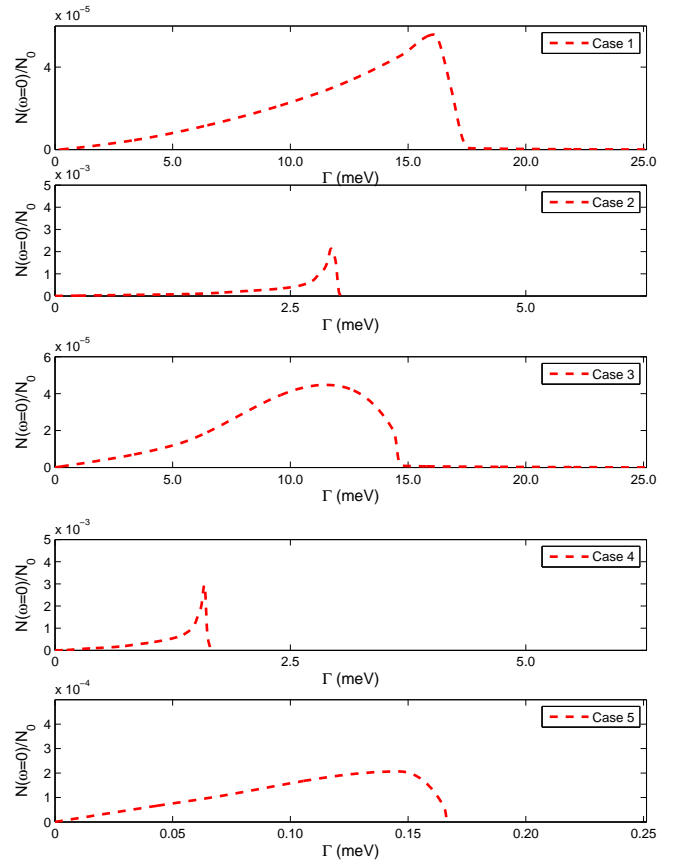

FIG. 2: Residual density of states $N(\omega = 0)$ normalized to the total normal state density of state at the Fermi energy N_0 vs. total unitary intraband scattering rate parameter Γ in meV. Figures (a)-(e) correspond to cases 1 to 5, respectively.

in the regime with nodes and no true gap in the system. The values of the scattering rate Γ for "dirty" systems presented here are chosen in each case to correspond to the maximum residual DOS induced by disorder as shown in Fig. 2. In all cases we have verified that the corresponding T_c suppression relative to the pure system is $\mathcal{O}(1\%)$ or less for all cases.

We note that for the various cases considered, the node-lifting process can take place at quite different rates. In particular, the nodes on the top of the closed Fermi sheet in case 5 are quite sensitive to a very small amount of disorder. The sensitivity of this case to disorder is the strongest argument against an explanation of the Reid *et al.* data based on a Fermi surface and state of type 5.

B. Penetration depth

The London penetration depth λ_i for currents flowing in the ith direction is a fundamental measure of the superconductivity and is related to the superfluid density by $\rho_s/m^* = (\mu_0 e^2 \lambda^2(T))^{-1}$. The superfluid density tensor is related to the total electromagnetic response of the

TABLE II: Zero temperature penetration depth.

Case	$\lambda_{0,ab}$ (nm)	$\lambda_{0,c}$ (nm)
1,2	87	334
3,4	87	287
5	87	329

system to an external field in the $\mathbf{q} \to 0, \omega = 0$ limit. For a general multiband dispersion $\epsilon_i(\mathbf{k})$ and in presence of the impurities, one finds that the penetration depth is given by the expression

$$
\begin{aligned}
\frac{1}{\lambda_\alpha^2} &= \frac{2\mu_0 e^2}{d\hbar^2} \sum_i m_i \int_0^\infty \frac{d\omega}{\pi} \left\langle \tanh\left(\frac{\omega}{2T}\right) \right. \\
&\times \left[(\mathbf{v_{F,i}}.\hat{\alpha})^2 \mathrm{Im}\left(\frac{\tilde{\Delta}_i^2}{(\tilde{\Delta}_i^2 - \tilde{\omega}_i^2)^{\frac{3}{2}}} \right) \right. \\
&- \left. \left. 2(\mathbf{v_{F,i}}.\hat{\alpha}\mathbf{v_{\Delta,i}}.\hat{\alpha}) \mathrm{Im}\left(\frac{\tilde{\Delta}_i \tilde{\omega}_i}{(\tilde{\Delta}_i^2 - \tilde{\omega}_i^2)^{3/2}} \right) \right] \right\rangle_{\phi,\mathbf{k}_z}
\end{aligned}
\tag{5}
$$

where d is the distance between planes, the index i denotes the band and α stands for the current direction ab or c and $\langle \ldots \rangle_{\phi,k_z}$ is an average over the Fermi surface. In the absence of disorder, this expression reduces to the result for the superfluid density of a clean system with general band found, e.g. in Ref. 41. The second term in Eq. (5) contains the nodal gap slope $v_\Delta \equiv \partial\Delta_\mathbf{k}/\partial\mathbf{k}$, which is extremely small compared to the Fermi velocity, and will be neglected in our calculations. Most experiments measure the change in the penetration depth $\Delta\lambda$ from some minimum temperature T_{min}, and are not sensitive to the absolute value of the penetration depth.

Note that since we begin from a realistic Fermi surface and assume a $T_c \sim 25K$ as appropriate for the Co-doped 122 systems, the reader might assume that we are in a position to calculate on an absolute length scale the zero temperature penetration depth λ_0. Indeed the expression (5) reduces at $T = 0$ to

$$
\frac{1}{\lambda_0^2} = \frac{2\mu_0 e^2}{\hbar^2 d\pi} \sum_i \langle m_i^* v_{F,i}^2 \rangle_{FS}
\tag{6}
$$

which gives the correct result in the limit of a single parabolic band. However a closer examination of Eq. (5) reveals that the integrand determining λ_0 extends over all occupied bands, i.e. it involves the full electronic structure and not just the Fermi velocities, whereas in Eq. (5) we have linearized the band structure near the Fermi level for simplicity. Thus we are not able to use Eq. (5) to obtain accurate estimates of λ_0 even if the input band structure $\epsilon_i(\mathbf{k})$ was perfectly correct. By contrast, the integrand determining

$$
\Delta\lambda_\alpha(T) \simeq \frac{\lambda_{0,\alpha}}{2} \left[\left(\frac{\lambda_{0,\alpha}}{\lambda_\alpha}\right)^2 - 1 \right]
\tag{7}
$$

is sharply peaked at the Fermi level, and so may be calculated accurately. Even in this case, however, the overall scale is set by $\lambda_{0,\alpha}$. The usual procedure would be to take $\lambda_{0,\alpha}$ from optical experiments. Indeed, in these systems the ab-plane penetration depth is of order 200-450 nm[42–47], but there are no reported measurements of $\lambda_{0,c}$ of which we are aware. For purposes of this work we use λ_0's determined from Eq. (6) (given for completeness in table II) to fix the scale of $\Delta\lambda_\alpha$. The overall length scale of field penetration may therefore be incorrect by up to a factor of two, but the T-dependence should be calculated accurately.

The temperature correction $\Delta\lambda(T)$ is often used as a probe of the nodal structure of gaps in unconventional superconductors[48]. In general, the asymptotic $T \to 0$ power laws for systems with line nodes are $\Delta\lambda \sim T$ for a clean and $\Delta\lambda \sim T^2$ for a dirty system[49], but the range of validity of these results may be experimentally unobservable depending on the form of the impurity scattering and the detailed momentum dependence of the superconducting gap. In our current calculations with intraband impurity scattering only, the concentrations have been chosen in order to minimize T_c suppression; the corresponding density of states and size of the asymptotic T^2 terms are therefore quite small, and the latter is not clearly visible in Fig. 3. On the scale of the Figure shown, these asymptotic power laws are modified by low energy scales associated with both sheets S_1 and S_2, as well as the significant energy dependence of the impurity self-energy. Over an experimentally relevant T range, a wide range of "best fit" power laws are therefore a priori possible.

In Fig. 3, we show $\Delta\lambda$ as a function of temperature for the various cases we consider here. The size of the observable quantity $\Delta\lambda$ is seen to be in reasonable agreement with the measured penetration depth changes in recent measurements in optimal to overdoped Ba-122[28]. The scale of $\Delta\lambda_c$ is significantly larger than $\Delta\lambda_{ab}$, due to the much larger $\lambda_{0,c}$. In addition, Figure 3 shows qualitatively different behavior for ab-plane and c-axis penetration depths. These results, particularly those for cases 3 and 4, are in qualitative agreement with experimental measurements on Ni doped 122 compounds, where linear T behavior along the c-axis and power law behavior for ab-plane with exponent $1.6 - 2.5$ for concentrations $x=0.03$ to 0.07 (only those above $x \sim 0.04$ are outside the spin density wave (SDW) state)[20] were reported. For Co doped 122 systems, we are not aware of any c-axis penetration depth measurements.

The ab-plane penetration depth data in 122 systems has been reported for some time now to be close to a power law T^α with an exponent α of about 2. It has usually been assumed that this result is obtained due to impurity scattering, either in a nodal system[18] or in a fully gapped $s_\pm$ state with interband scattering such that midgap bound states are formed[50]. These effects may indeed be present in very dirty samples. However, the existence of a linear-T term for the c-axis penetration depth suggests that this simple argument cannot be the
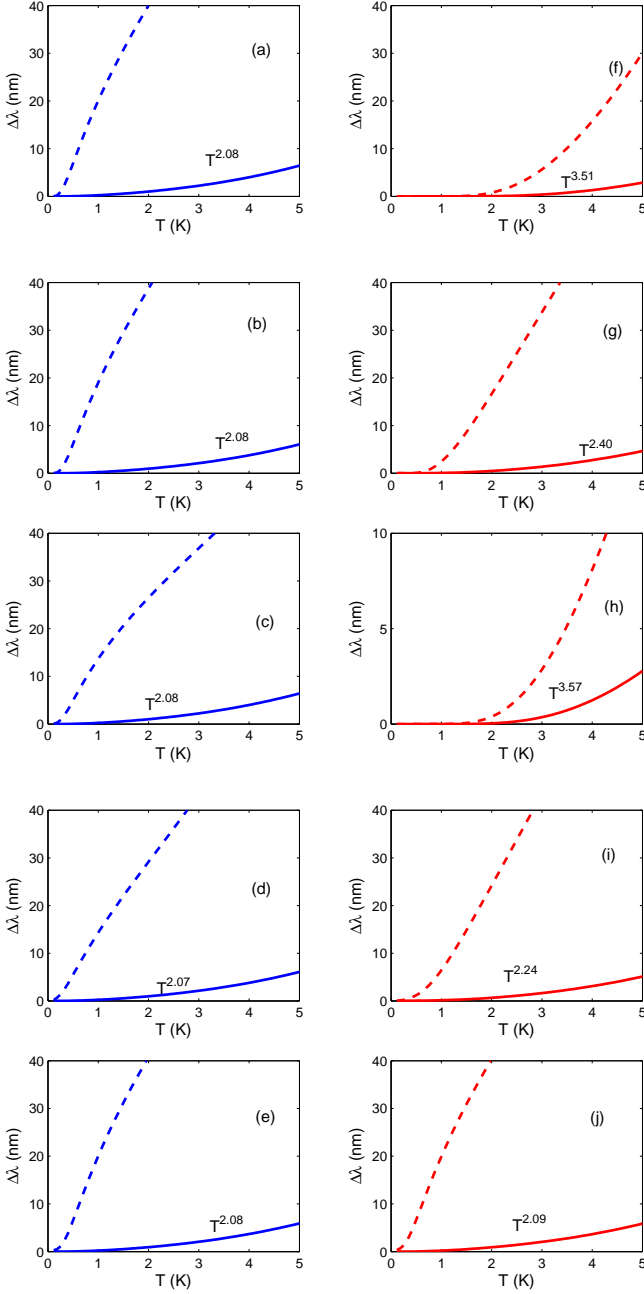
FIG. 3: Change in penetration depth $\Delta\lambda$ measured in nm vs. temperature T. Panels (a)-(e): clean penetration depth for c-axis (dashed lines) and ab-plane (solid lines) currents for cases 1-5. (f)-(j): same plots for dirty system with Γ chosen in each case to give the maximum $N(\omega = 0)$ in Fig. 2. For λ_{ab}, power laws over the T range shown in the panel are indicated.

complete explanation for the approximate T^2 behavior in the better samples; were the system sufficiently dirty to show T^2 behavior in the ab-plane, it would perforce manifest the same behavior for currents in the c-axis direction (we ignore for the moment the possibility that impurity scattering is itself highly anisotropic with respect to the ab/c directions.). The difference in power laws in the two

directions must therefore be ascribed to some other effect or combination of effects. In our proposal, there is no true T^2 behavior except perhaps at the very lowest temperatures; the upward curvature observed over a range of several Kelvin is due in part to the "activation" of a new source of quasiparticle excitations as the temperature is increased. At low temperature all quasiparticles come from sheet S_1, since we have assumed that this is the only sheet where true nodal excitations exist. On the other hand the order parameter on the S_2 sheet is assumed to have deep minima Δ_{min}. When T exceeds this scale, quasiparticles from this sheet may be excited and a new contribution (upward curvature) to $\Delta\lambda$ appears. Since S_2 is assumed to have smaller $v_{F,c}$, it does not contribute significantly to $\Delta\lambda_c$, however. The second cause of "power law" behavior is indeed the disorder, but it is impossible to make universal statements about the large T ranges over which experiments are typically fit. To give a more useful measure of the form of these results in Fig. 3, we have performed best fits of the T dependence to $\Delta\lambda \sim T^\alpha$ over the finite range of temperatures shown.

The penetration depth anisotropy

$$\gamma_\lambda \equiv \frac{\lambda_c}{\lambda_{ab}} \simeq \frac{\lambda_{0,c}}{\lambda_{0,ab}} \left(1 + \frac{\Delta\lambda_c}{\lambda_{0,c}} - \frac{\Delta\lambda_{ab}}{\lambda_{0,ab}}\right) \qquad (8)$$

has been claimed in Refs. 51,52 to be of order 3-6 at low temperature, and to decrease weakly with increasing temperature, but cannot yet be measured directly. Experimentally, $\Delta\lambda_i$ is measured, and must be combined with measurements of $\lambda_{0,i}$, with $i = c, ab$ to determine the anisotropy ratio. Reliable measurements of $\lambda_{0,c}$ from, e.g. optics experiments, are not yet available for the 122 materials to our knowledge. However, within our theoretical framework γ_λ can be determined, with the caveats described above, and Fig. 4 shows γ_λ for the different cases. We therefore regard this as a prediction of weakly increasing γ_λ with temperature which may be verified at the point that reliable values of $\lambda_{0,c}$ are obtained from optics or elsewhere. Our results are in the range of anisotropy ratios deduced from experiment[51], but increase weakly rather than decrease weakly with temperature at low temperatures. A glance at the approximate inequality in Eq. (8) shows that a somewhat smaller value of $\lambda_{c,0}$ than effectively assumed in Refs. 51,52 would bring the measured $\Delta\lambda_i$'s and therefore the T-dependence of γ_λ in agreement with our results.

We can now ask which type of Fermi surface/order parameter combination represents the experimental penetration depth data best. For cases 1 and 2, the c-axis Fermi velocity is small, which means not only that $\Delta\lambda_c$ is smaller at low T, where it derives entirely from the S_1 nodes, but also that the contribution from the S_2 deep minima is correspondingly more important; as seen in Fig. 3, for these cases the c-axis penetration depth as a function of T has substantial upward curvature, which is never observed in experiment. Power law fits to the ab-plane results give exponents which tend to be too close
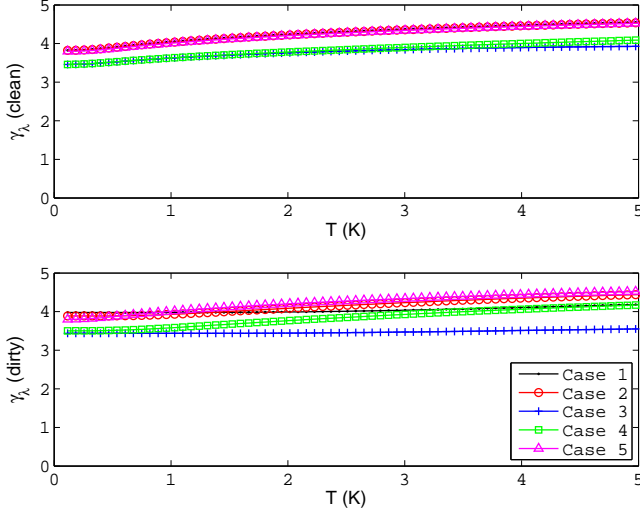
FIG. 4: Penetration depth anisotropy $\gamma_\lambda (= \lambda_c/\lambda_{ab})$ as a function of temperature. Top: clean systems with $\Gamma = 0.0$. Bottom: dirty systems with Γ chosen as in Fig. 3.

to 1. On the other hand for cases 3 and 4, $\Delta\lambda_c(T)$ has no upward curvature above a scale corresponding to approximately $1K$ and is quasilinear over a significant T range, while $\Delta\lambda_{ab}(T)$ displays power law behavior with α approaching 2 in the dirty cases shown over a finite range, as observed in experiment. Case 5 displays a large penetration depth anisotropy, but an anomalous T dependence which is due to the extremely small Δ_{min} for this case which must be chosen to place the nodes in a position with high $v_{F,c}$. Therefore from the point of view of the penetration depth temperature dependence and crude anisotropy, only cases 3 and 4 appear compatible with experiment. We emphasize again that the power laws stated in Fig. 3 are phenomenological fits and are not exact in any asymptotic limit. Exponents may be expected to change as the low energy gap scales are changed, and in particular to increase somewhat as interband scattering is added.

Before closing this section, we note that nonlocal electrodynamics are unlikely to play a significant role in these measurements. This is because the typical energy scale which cuts off singularities in nodal superconductors is $E^\alpha_{nloc} \equiv (\xi_\alpha/\lambda_\alpha)\Delta_0$. For both directions in the 122 samples, this scale is of order a few tenths of Kelvin or less. The crossover in clean samples from linear T to T^2 from nonlocal effects will therefore only complicate interpretations at unobservably low temperatures, where disorder will probably dominate in any case.

C. Thermal conductivity in zero magnetic field

The electronic thermal conductivity κ is calculated here using a straightforward extension of the standard approach[53–55] to multiband superconductors[18]. In the presence of disorder, we evaluate the expression arising from the electronic heat current bubble,

$$\frac{\kappa_\alpha}{\kappa_n} = \frac{3}{4\pi^2 T_c \sum_i \langle m_i(\mathbf{v}_{\mathbf{F},\mathbf{i}}.\hat{\mathbf{a}})^2/\Gamma_i\rangle_{\phi,k_z}} \sum_i \int_0^\infty d\omega \qquad (9)$$

$$\left\langle \frac{m_i}{\mathrm{Re}[\sqrt{\tilde{\Delta}_i^2 - \tilde{\omega}_i^2}]} \left(v_{i-}^2 + \frac{|\tilde{\omega}|_i^2 v_{i+}^2 - |\tilde{\Delta}|_i^2 v_{i-}^2}{|\tilde{\omega}_i^2 - \tilde{\Delta}_i^2|} \right) \right\rangle_{\phi,k_z}$$

$$\times \ \mathrm{sech}^2\left(\frac{\omega}{2T}\right)\frac{\omega^2}{T^2},$$

where

$$\kappa_n = \frac{\pi}{12}\frac{nk_B^2 T_c}{\hbar d}\sum_i \langle m_i(\mathbf{v}_{\mathbf{F},\mathbf{i}}.\hat{\mathbf{a}})^2/\Gamma_i\rangle_{\phi,k_z} \qquad (10)$$

and $\alpha = a, c$, m_i is the band mass, $\mathbf{v}_{F,i}$ is the Fermi velocity on the ith band, and $v_{i\pm}^2 \equiv v_{F,i}^2 \pm (\partial_\alpha\Delta_{\mathbf{k},i})^2$. Terms involving the gap slope v_Δ at the nodes are numerically negligible since $v_\Delta \ll v_F$ and are omitted in our evaluations. Here, $\langle \ldots \rangle_{\phi,k_z}$ is an average over each Fermi surface sheet, $\sum_i$ denotes the sum over the bands, $v_{F,i}$ is the Fermi velocity on sheet i, and n is the number of FeAs planes per unit cell.

We focus first on the linear term in κ in the $T \to 0$ limit, the only experimentally unambiguous signature of purely electronic heat transport by nodal excitations. In the limit $T \to 0$, Eq. (9) reduces to

$$\frac{\kappa^i}{T}\Big|_{T\to 0} \simeq aN_{\mathrm{nodes}}\frac{k_B^2 m^*}{\hbar d}\left[\frac{v_{F,i}^2}{k_F v_{\Delta,i}}\right]_{\mathrm{node}}, \qquad (11)$$

where a is a dimensionless constant, N_{nodes} is the number of distinct nodal surfaces, assumed equivalent, and m^* is the effective mass for motion of quasiparticles in the ab-plane. The result obtains exactly only if $v_{F,i}$ and $v_{\Delta,i}$ are constant over the entire nodal surface, which is unrealistic except, crudely speaking, in a 2D situation, but if the velocities are replaced by the average expression of Eq. (11) will give a reasonable result. The constant a reduces to $1/6$ in the well-known case of a 2D d-wave order parameter, and will be of the same order of magnitude for a clean nodal $s_\pm$ state if the nodes are vertical and run the length of the Fermi cylinder. In any situations where the nodal lines do not span the dimensions of the Fermi sheet, i.e. consist of small circles or segments, as in all the cases for S_1 considered in Fig. 1, the factor a contains the relative nodal phase space and will therefore be $a \ll 1$. Note that in the d-wave and certain p-wave cases, the result of Eq. (11) is also universal, in the sense that the nodal velocities are unrenormalized by disorder[23,24], but in the generalized $s_\pm$ case this universality breaks down[18].

It is instructive to compare crude estimates of what one might expect for $\lim_{T\to 0}\kappa_i/T$ with actual theoretical results and the experimentally measured values. In

TABLE III: Theory columns: comparison of different estimates of the $T \to 0$ limit of Eq. (9) for currents in the ab-plane, expressed in $\mu W/K^2 cm$ for a system with T_c=23K and $d = 13$Å, with Fermi velocities and order parameters for the various cases as given in Sec. II A. Method T1: 2D d-wave universal result using $\langle v_F \rangle_{rms}$ from Table I and $k_F \langle v_\Delta \rangle_{rms} \sim 2k_B T_c$ and $a = 1/6, N_{nodes} = 4$ in Eq. (11); Method T2: Eq. (11) using $\langle v_{F,a} \rangle_{rms}$ and $\langle v_\Delta \rangle_{rms}$ averaged over the nodal manifold for each case. Method T3: Full numerical result from Eq. (9). Ba(Fe$_{1-x}$Co$_x$)$_2$As$_2$: Experimental data for asymptotic low-T linear-T term in κ_{ab} from Ref. 21 for values of x shown. Numbers in parentheses are values of extrapolated linear term in $\mu W/K^2 cm$ for different samples; zero is reported if these are negative. LFPO: value for LaFePO from Ref. 56; P-122 value for BaFe$_2$(As$_{1-x}$P$_x$)$_2$ with x=0.33 from Ref. 57

	Theory			Ba(Fe$_{1-x}$Co$_x$)$_2$As$_2$				LFPO	P-122
Case	T1	T2	T3	0.074	0.108	0.114	0.127		0.33
1	118	31	1.8						
2	118	71	3.1						
3	102	31	2.5	0	0	0	17	3000	250
4	102	59	6.3	(-1,3)	(-1)	(-9,-13)			
5	94	47	3.1						

Table III we first show progressively more accurate estimates of this quantity. First, we remark that a small linear-T term in κ_{ab} *must* be present if nodes are present and if $\mathbf{v}_F$ has any nonzero component in the ab-plane. To be consistent with earlier data and with the recent work of Reid *et al.*[21] in the Co-doped Ba-122 system, this term must be quite small, consistent with zero within the resolution of the experiment, at least near optimal doping. It is clear from the table that a 2D d-wave state or, equivalently, an anisotropic nodal s-wave state with line nodes running the length of the Fermi cylinder ("method T1") would dramatically overestimate the experimental results for κ/T in the ab plane. The best estimate based on Eq. (11) ("method T2"), accounting for realistic values of nodal velocities v_Δ, still gives a value significantly larger than experiment near optimal doping in the Ba(Fe$_{1-x}$Co$_x$)$_2$As$_2$ system studied by Reid *et al.* as shown in Table III. This is at least in part because method T2 also does not account for the small nodal phase space. The T3 column of Table III shows the clean limit of the exact numerical evaluation of Eq. (9) for the 5 cases. These results are now of order the scatter in the data (consistent with zero) of the ab-plane linear-T terms in κ identified in samples near optimal doping by Reid *et al.*, which we take to be the resolution of the experiment, about $\sim 1\mu W/K^2 cm$.

Depending on the Fermi surface, the corresponding c-axis transport can be smaller or larger than the ab-plane results discussed. To illustrate the qualitative anisotropy found here, we plot in Fig. 5 the ab-plane and c-axis thermal conductivities κ/T for increasing intraband impurity scattering. There are several interesting points in this Figure. First, we note that for cases 1 and 2, where
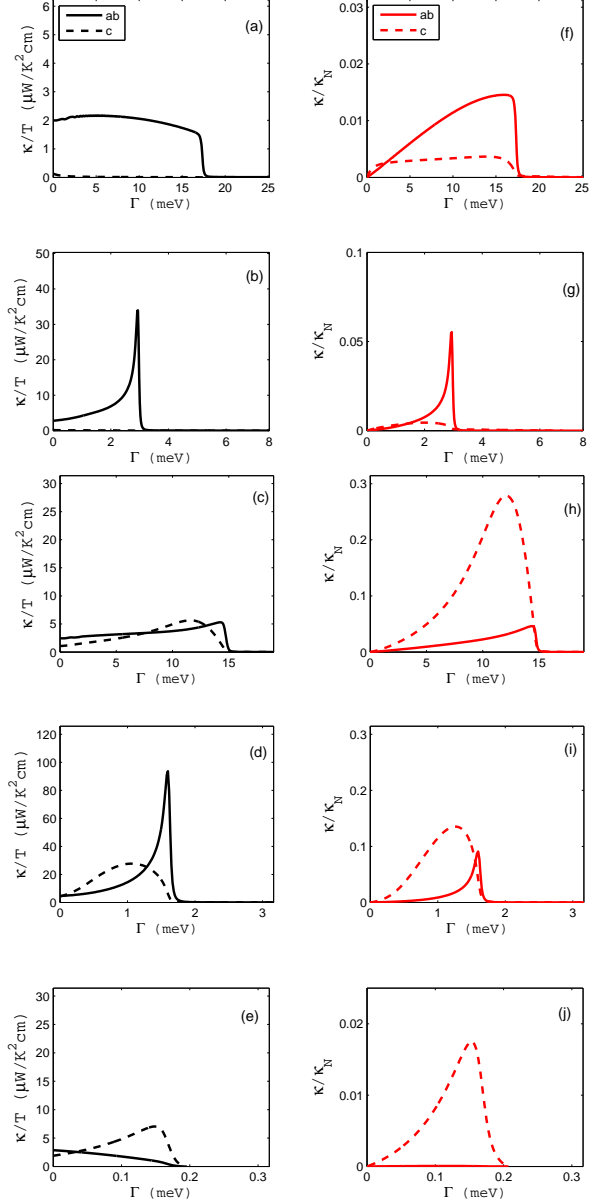

FIG. 5: Residual thermal conductivity $\lim_{T\to 0} \kappa(T)/T$ in units of $\mu W/K^2 cm$ as a function of impurity scattering rate Γ in meV. Panels (a,c,e,g,i) correspond to absolute thermal conductivity for thermal current in the ab-plane (solid) and along the c-axis (dashed), respectively, for cases 1-5 depicted in Fig. 1. Panels (b,d,f,h,j) correspond to normalized thermal conductivity κ/κ_N for the same cases.

the Fermi surfaces are nearly cylindrical, the ab-plane conductivity is much larger than the c-axis conductivity. Clearly again these cases are inconsistent with experiment. For the more flared Fermi surface, cases 3 and 4, it is possible to have κ_{ab}/T and κ_c/T comparable, or even have $\kappa_c > \kappa_{ab}$. Note this is more likely for the horizontal line nodes of case 4, which have been chosen to lie at the maximum value of $v_{F,c}$ for this Fermi surface, whereas
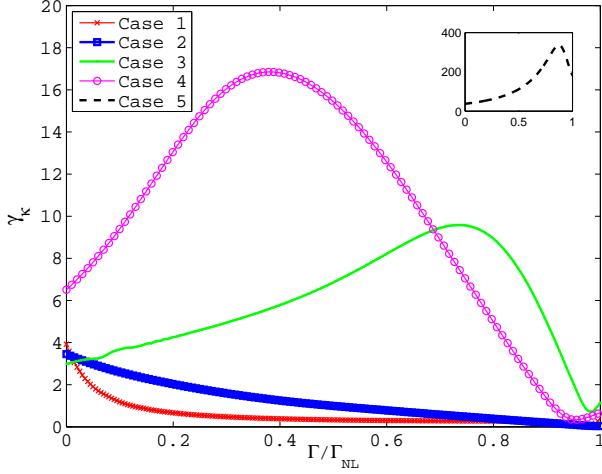
FIG. 6: Normalized thermal conductivity anisotropy ratio $\gamma_\kappa = \lim_{T\to 0}(\kappa_c/\kappa_{c,N})/(\kappa_{ab}/\kappa_{ab,N})$ as a function of the disorder scattering rate normalized to the critical value of disorder Γ_{NL} that lifts the nodes.

the V-shaped nodes of case 3 sample the high $v_{F,c}$ values less often. A large c/a anisotropy is also observed in case 5 for reasons similar to those of case 4.

As intraband scattering is increased, a constant term is added to the off-diagonal self-energy in Nambu space[18] which eventually lifts the nodes, as seen in the DOS (Fig. 2). As this occurs, two effects happen in parallel: a) v_Δ decreases; and b) the nodal surfaces (which are shown in Fig. 1 for the clean system only) move towards the top and bottom of the Brillouin zone, respectively. The latter effect can increase or decrease the thermal conductivity depending on whether or not the node-lifting process moves the nodes towards regions of higher or lower $v_{F,c}$. Thus, depending on details, the c/a anisotropy can be enhanced or suppressed by disorder.

In Ref. 21, the authors specifically discuss the *normalized* measure of thermal conductivity anisotropy $\gamma_\kappa \equiv \lim_{T\to 0}(\kappa_c/\kappa_{c,N})/(\kappa_{ab}/\kappa_{ab,N})$, and demonstrate that this ratio has a minimum at optimal doping. This result should be treated with caution, however, both because a) the linear term in κ_{ab} is consistent with zero for much of the doping range; and b) the normal state κ_N's are determined by measurement of the resistivity extrapolated to $T = 0$ and use of the Wiedemann-Franz law. However, if the elastic transport scattering rate $1/\tau_{tr}$ is reasonably isotropic, as seems likely, γ_κ will be determined simply by the ratio

$$(\langle v_{F,c}^2\rangle_{\text{node}}/\langle v_{F,c}^2\rangle)/(\langle v_{F,ab}^2\rangle_{\text{node}}/\langle v_{F,ab}^2\rangle), \quad (12)$$

where $\langle v_{F,\alpha}^2\rangle_{\text{node}}$ is the average of the Fermi velocity components α over the nodal manifold. Here we calculate γ_κ within a simple model where normal state heat conduction is controlled by (isotropic) intraband impurity scattering only. In Fig. 6, we show that only for cases 3-5 it is possible to achieve values of γ_κ substantially greater than 1. For case 5, the node lifting scattering

rate Γ_{NL} is minuscule in absolute units, such that we rule out this case as well, provided our assumption that intraband scattering dominates is correct.

An alternate possibility to create a small residual κ/T would be the creation of an impurity band in a gapped state due to interband scattering[18], but in this case there is no natural reason to have a transport anisotropy other than that given by $\kappa_c/\kappa_{ab} \sim \langle v_{F,c}^2\rangle/\langle v_{F,ab}^2\rangle$, which for all cases discussed here would give a very strong dominance by the ab-plane thermal currents on an absolute scale, and would lead to $\gamma_\kappa \simeq 1$ in all samples, in contrast to experiment.

D. Magnetic field dependence of κ

The final notable feature seen in experiment[17,21] is an unexpectedly large enhancement of the in-plane residual κ/T term in the presence of a magnetic field along the c-axis. With moderate magnetic field of a few Tesla, the residual in-plane term $\kappa_{ab}(H, T \to 0)/T$ becomes comparable to the c-axis term $\kappa_c(H, T \to 0)/T$, and both exhibit a field dependence with downward curvature reminiscent of the presence of field-induced residual quasiparticle excitations contributing to the thermal current[58]. This effect was discussed already for the ab-plane thermal conductivity in Ref. 18, where it was concluded that the most likely origin of the strong field dependence in apparently fully gapped samples was contributions from deep minima in the gap on the electron sheets, as found in early multiorbital spin fluctuation theories[7,10,12,13,59]. Note that in the 3D spin fluctuation analysis of Graser *et al.*[26], these deep minima on the electron sheets continue to exist, and run the entire length of the Fermi cylinders, thus providing much more phase space than at zero field, as soon as the magnetic field energy spans the very small minimum gap Δ_{min}. Thus the ab thermal conductivity, negligible in zero field, can jump fairly rapidly[39].

To include the presence of magnetic field explicitly, in this work we use the standard semiclassical (Doppler shift) method[58,60–62], where the quasiparticle energy is modified by its Doppler shift in the local superfluid flow field. While this approach is never exact[63], it provides a good qualitative description of the magnetic field dependence of the quasiparticle properties of nodal superconductors over a wide field range[64]. The local Doppler shift of a quasiparticle with momentum $\mathbf{k}$ (band indices are suppressed) is

$$\delta\omega(\mathbf{k},\mathbf{r}) = \mathbf{v}_F(\mathbf{k})\cdot\mathbf{p}_s(\mathbf{r}) \quad (13)$$

where $\mathbf{p}_s(\mathbf{r})$ is the local supercurrent momentum, approximated for a single vortex as

$$\mathbf{p}_s(\mathbf{r}) = \frac{\hbar}{2r}\hat{\theta} \quad (14)$$

Here r is the distance from the vortex core and θ is the vortex winding angle. In the presence of the magnetic
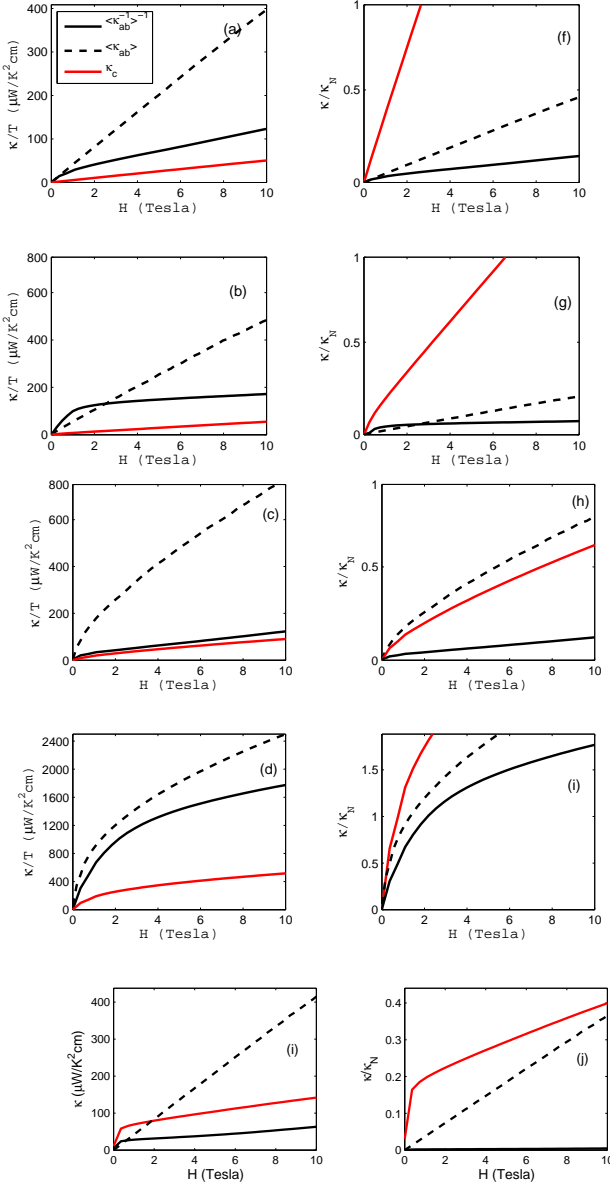
FIG. 7: Residual thermal conductivity κ/T in units of $\mu\text{W/K}^2\text{cm}$ vs. magnetic field H in Tesla. Panels (a)-(e): cases 1-5 for Fermi surface S_1 with intraband scattering rate $\Gamma = 1.3$ meV (Case 1), $\Gamma = 0.6$ meV (Case 2) and $\Gamma = 1.9$ meV (cases 3,4), and $\Gamma = 0.06$ meV for case 5.

field, we replace $\tilde{\omega}$ by $\tilde{\omega} - \delta\omega(\mathbf{k}, \mathbf{r})$ in Eq. (9). In this approach, any physical quantity is calculated in the usual way with Doppler shifted energy, and the averaging is performed over a unit cell of the vortex lattice, approximated as circular, as

$$\kappa(H) = \frac{1}{\pi R_H^2} \int_0^{R_H} dr \, r \int_0^{2\pi} d\theta \kappa(\mathbf{r}), \qquad (15)$$

where $\kappa(\mathbf{r}, \theta)$ is the local (Doppler shifted) result from Eq. (9), $R_H = \sqrt{\Phi_0/\pi H}$ is the magnetic length scale, with Φ_0 the superconducting flux quantum. For lower

fields $H \ll H_{c2}$, this is a qualitatively good approximation. Somewhat more sophisticated approximations can be obtained within the semiclassical framework[62], but the above will suffice for our qualitative purposes. Here $H_{c2} \equiv \Phi_0/(2\pi\xi_0^2)$ is the upper critical field and $\xi_0 = v_F/(2\pi T_c)$ is the coherence length.

Using this method, we now calculate the low-T residual thermal conductivity in both directions as a function of the magnetic field. Fig. 7 shows the field dependence of the residual linear term, which is similar to a superconductor with nodes, for both directions of the heat current, with the magnetic field taken always to point along the c-axis as in experiment. Note that in principle the situations with heat current parallel and perpendicular to the field are physically different regardless of the orientation of the crystal axes: in one case the heat current flows down the axis of a vortex and may be assumed to sample a single $\kappa(\mathbf{r})$, while in the other case it samples a modulated $\kappa(\mathbf{r})$ across the vortex lattice. This averaging problem for the perpendicular heat flow has never been addressed in a completely convincing fashion. We therefore present two extremes of the possible field dependence for currents in the the ab-plane: first, a "parallel average" over the vortex flow field $\langle\kappa_{ab}\rangle \equiv \langle\kappa(\mathbf{r})\rangle$, where $\langle...\rangle$ represents a direct average over the vortex unit cell as in Eq. (15); second, a "series average", $\bar{\kappa}_{ab} \equiv \langle\kappa(\mathbf{r})^{-1}\rangle^{-1}$, as discussed in Ref. 58. We note that the results for the Brandt-Pesch-Tewordt average Green's function theory[39] appear to lie closer to the parallel average.

Fig. 7 shows several interesting effects. First of all, while the Fermi surfaces with less flaring (cases 1 and 2) displayed much larger values of the absolute ab-plane thermal conductivity in zero field (Fig. 5, panels (a) and (b)) than the more flared cases 3 and 4 (Fig. 5, panels (c) and (d)), the ab-plane field dependence $\kappa_a(H)$ at any reasonable field is seen to dominate the absolute c-axis response $\kappa_c(H)$ for all cases 1-4 (Fig. 7, panels (a-d)). This is because we have assumed, as in Ref. 39, that the S_2 sheet has a deep gap minimum, spanned by the Doppler field energy E_H at a field H of only 1.2 T. Note this is an average scale over the entire sheet; the dispersion of the Fermi velocity with k_z leads to a smearing of any feature associated with this scale. It is these long deep gap minima on S_2 (putative electron sheets) which dominate the field response in this case, with subdominant contributions from the S_1 (putative hole sheets) above this field range. Because $\kappa_{cN} \ll \kappa_{aN}$, it is still possible to have a normalized thermal conductivity larger in the c-axis direction (Fig. 7, panels (f) and (g)).

The Reid $et~al.$ experiment Ref. 21 shows a pronounced tendency for the normalized anisotropy ratio γ_κ to fall rapidly from large values as a function of magnetic field, and then to saturate at values of order 1 when fields of a few Tesla are reached. Within our calculational scheme, such a conclusion is quite natural since the zero-field anisotropy (Fig. 6) γ_κ is dominated by the weak nodes on the S_1 sheet(s), which can give large γ_κ's, particularly in cases 3 and 4, as discussed above. On the other hand,
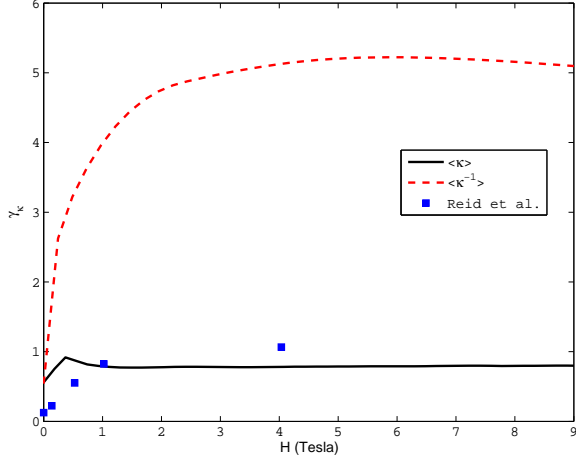
FIG. 8: Inverse normalized thermal conductivity anisotropy ratio $\gamma_\kappa^{-1} = \lim_{T\to 0}(\kappa_a/\kappa_{a,N})/(\kappa_c/\kappa_{c,N})$ a function of magnetic field for Case 3. Solid line: parallel averaging $\langle\kappa_{ab}\rangle$; dashed line: series averaging $\langle(\kappa_{ab}^{-1})\rangle^{-1}$ as described in text. Symbols: $\langle(\kappa_{ab}^{-1})\rangle^{-1}$ data for highly overdoped $x = 0.127$ sample of Ref. 21, which shows nonzero κ_{ab}/T as $T \to 0$.

as the field is switched on, the contributions of the deep gap minima on the S_2 sheets come into play, and indeed dominate for sufficiently large fields because of the much larger phase space of the gap minima on S_2 compared to the phase space taken by the gap nodes on S_1. If a single 2D sheet dominates the field dependence, the normalized anisotropy ratio will reduce to approximately 1 since the Fermi velocity anisotropy has been removed by the normalization, *provided* the averaging over the vortex lattice is performed identically for in-plane and c-axis currents. This behavior is seen in Figure 8, where the inverse of the anisotropy ratio, γ_κ^{-1} is plotted to facilitate comparison with experiment. If series-type averaging is more appropriate in the ab-plane, the high-field γ_κ^{-1} can be considerably larger, as also seen in Figure 8.

E. Doping dependence

Within our current crude approach, doping is accomplished by rigidly shifting the chemical potential relative to the parent compound. However, the dependence of the Fermi surface thus obtained is consistent neither with that observed in ARPES experiments on 122 compounds nor with virtual crystal approximation within DFT calculations. In particular, the flaring of the hole (S_1) Fermi surface upon electron doping does not increase rapidly with electron doping, as seen in ARPES and DFT calculations[33,36]. In this section we therefore investigate, independently of any microscopic model of the band structure, the effect on superconducting state transport of the flaring of the S_1 Fermi surface. To this end, we simply interpolate the Fermi surfaces between cases (1,2) and (3,4), and calculate the thermal conduc-
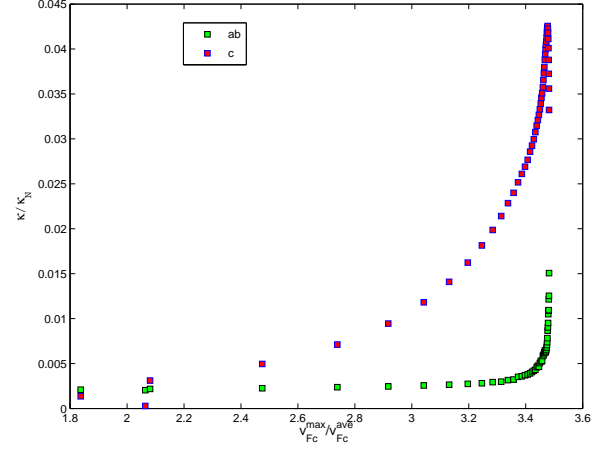

FIG. 9: Normalized thermal conductivity κ/κ_N for heat current in a and c directions vs. degree of flaring of Fermi surface S_1, parametrized by v_F^{max}/v_F^{ave}.

tivity as outlined above. The superconducting order parameter is held fixed in this process. Within our current interpretation of the data on Co-doped Ba-122, increasing the amount of flaring is equivalent to doping the system, although the correspondence between the two scales is nonlinear and not completely determined. Nevertheless, it is clear that an essential feature of the experiment, the strong increase of the normalized anisotropy ratio γ_κ can be understood by making this simple assumption. Note that the normalization automatically divides out the average effect of the increasing $v_{F,c}/v_{F,ab}$; what happens, therefore, is that the flaring increases particularly near the nodes and therefore preferentially enhances low-energy c-axis quasiparticle transport. Fig. 9 illustrates the effect of the increased flaring, parameterized by the ratio of the Fermi velocity components, for the order parameter with V-shaped nodes as in cases 1,3. The effect is superficially quite similar to the effect of doping on the anisotropy ratio observed by Reid *et al.*[21].

F. Modulations of κ with respect to magnetic field angle

Measurements of the specific heat and thermal conductivity as a function of the angle between an applied magnetic field and the crystal axes are in principle powerful methods to determine the location of gap nodes[61,65]. Since these measurements are probes of the bulk properties, and the treatment of surfaces in the Fe-pnictide systems continue to pose problems, rotating field measurements were proposed early on as appropriate ways to map nodal structures of the order parameter in these systems[66]. Measurements of the low temperature specific heat as a function of the angle of an in-plane magnetic field have been reported very recently[67]. While this method is sensitive to vertical line nodes, it misses hor-
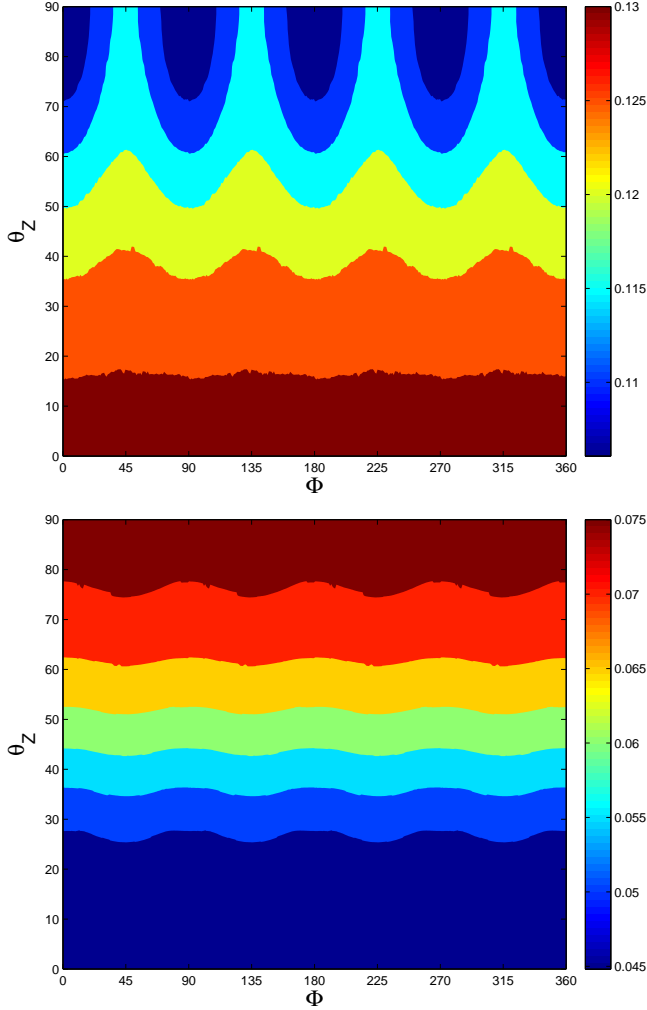
FIG. 10: Residual specific heat $C(\mathbf{H})/C_N$ (top) and c-axis thermal conductivity (bottom) $\kappa_c(\mathbf{H}, T \to 0)/\kappa_{cN}$ normalized to zero field normal state values as a function of direction of applied magnetic magnetic field described by polar angle θ_Z and azimuthal angle Φ. The Fermi surface and form of order parameter used for this calculation is same as case 3 with $\Delta_h = 0.3meV$ and $\Delta_e = 1.3meV$. Magnetic field strength is $10.0T$.

izontal nodes altogether and can also miss nodal structures near the extrema of the Brillouin zone for a flared Fermi surface. Similar considerations apply to the oscillations of the thermal conductivity with field angle, which historically have been more sensitive to weak nodal structures. Here we have calculated, for an arbitary direction of the magnetic field, the thermal conductivity for a fixed amplitude of the magnetic field for case 3.

The results of these calculations are shown in Fig. 10. The situation for polar angles θ_Z near zero, i.e. for an alignment of the field along the c-axis direction and the heat current applied with an in-plane angle Φ, clearly causes negligible thermal conductivity oscillation. As the polar angle is increased, the expected characteristic four-

fold oscillations emerge[68]. Since we have evaluated the conductivity at $T \to 0$, minima as a function of Φ for constant θ_Z reflect the existence of nodes at angles $90° - \theta_Z$. We have evaluated the T dependence as well, and find that inversions of this pattern can occur at higher T[68–70], but have not focussed on this aspect here. Within our model, for most angles the observed fourfold oscillations with minima at $0°$ and $90°$, correspond to the deep minima of the gap function on the S_2 sheet assumed in our model. Only when θ_Z approaches $90°$ are the nodal surfaces on S_1 probed by the field. One should expect for cases 1 and 3 (V-shaped nodes) new double minima on both sides of $\Phi = 0°$, $90°$, etc. to appear due to the V-shaped nodes for polar angles $\theta_Z \lesssim 90°$. These are not visible in the Figure, however, in part because the anisotropy of the Fermi surface masks small nodal features. In our model it appears difficult to observe these small features, but it may nevertheless be possible to detect them with high experimental resolution. Since the cases with full horizontal nodes are robust, one might think that a polar angle scan of the magnetic field would easily pick up minima due to these features, but this effect, while present, is obscured in our calculations by the c-axis dispersion of the Fermi velocity. Our study suggests that a careful mapping of the weak S_1 nodal structures with this method, while clearly desirable, may unfortunately be difficult both due to the small size of the related signals and of course the experimental implementation of the 3D field rotation.

IV. CONCLUSIONS

In the presence of an order parameter with 3D structure on an anisotropic FS, transport properties may be qualitatively very different along the plane and the c axis, and FS topology may also play an important role. In particular, the Fermi velocity is a characteristic weight factor for transport coefficients: a larger Fermi velocity near the high density of quasiparticles around gap nodes will greatly enhance the superfluid density, microwave or thermal conductivity. Our calculations, within the framework of anisotropic $s_\pm$ states found in recent spin fluctuation calculations[26] for 122 systems, support the suggestion of Reid $et\ al.$ that the anisotropy observed in the thermal conductivity at low T in 122 systems is most likely due to the occurrence of gap nodes on portions of the Fermi surface with large c-axis component of the Fermi velocity. It is noteworthy that from the point of view of microscopic theory, the nodal structures which dominate the c-axis transport in the Co-doped Ba-122 materials are most likely to be found on the hole rather than electron Fermi surfaces, in contrast to calculations appropriate for 1111 and other more 2D materials which found the opposite. It is also possible that changes in microscopic interaction parameters can lower the gap minima on the electron sheets so as to become nodes, as may occur in the P-doped 122 material. Our calculations are

phenomenological in nature and have only assumed that the nodes occur on one sheet of either type.

Linear-T terms in the thermal conductivity can arise whenever a finite density of residual quasiparticle states exists at the Fermi level due to a small amount of disorder. Some suggestions have been made that experiments indicating low-energy quasiparticle states can be understood by considering an isotropic $s_\pm$ state without nodes but with interband scattering, such that an impurity band is created at the Fermi level[71]. At least in the 122 systems, this possibility now appears to be conclusively ruled out, for several reasons. First, such an impurity band would lead to a dominant T^2 dependence of the penetration depth, not linear-T, as reported by Ref. 20 in 122 systems). Secondly, at low T disorder scattering is the dominant scattering mechanism and also determines the characteristic transport time. Calculations with realistic impurities show weak variation of the relaxation rate around the Fermi surface; and the density of impurity band states is therefore roughly isotropic; thus transport anisotropy will be determined in such a situation entirely by the ratio $\langle v_{F,c}^2 \rangle / \langle v_{F,ab}^2 \rangle \ll 1$, rather than by the Fermi velocity values on special parts of the Fermi surface. This result is now inconsistent with Ref. 21. For this reason we have neglected a treatment of interband impurity scattering in this work, but realistic calculations will require a knowledge of both intra- and interband scattering amplitudes of the dopant impurities.

In our work here we have also neglected magnetic impurities, in part because the microscopic calculations of Kemper et. al.[38] reported a weak magnetic potential component of the Co dopant. In addition, magnetic impurities are generically strong pairbreakers in A_{1g} states. Similar to the discussion of interband nonmagnetic scatterers above, if they were strong enough to form impurity bands on the Fermi level and thus influence transport, they would create significant T_c suppression, large values of the linear residual term in κ_{ab}, and a normalized anisotropy γ_κ in zero field close to unity, none of which are observed in experiment.

We have focussed here primarily on two properties, penetration depth and residual thermal conductivity in the $T \to 0$ limit. For two concrete examples of Fermi surfaces "inspired" by forms which occur in density functional theory calculations for certain 122 systems, we have shown that one can simultaneously explain the existence of large penetration depth and thermal conductivity anisotropies $\gamma_\lambda, \gamma_\kappa > 1$, indicating a predominance of nodal quasiparticles with large c-axis components of the Fermi velocity. Because of the complicated multiband nature of the system, as well as because the order parameters assumed have important low-energy minimum gap scales, asymptotic low T power laws will rarely be observed in the penetration depth $\Delta\lambda(T)$ if the T dependence is fit to an experimentally relevant range. We have therefore tried to give fits $\Delta\lambda(T) \sim T^\alpha$ to our theoretical results over such a finite range, and found for two promising cases with "flared" or closed Fermi surfaces in-plane exponents $\alpha_{ab} \gtrsim 1.5 - 2$ which depend on details of order parameter structure and on topology of Fermi surface. On the other hand, the c-axis penetration depth change is very close to linear T dependence for these cases. These results are quite close to those obtained in experiment by Martin et al.[20]. Quantitative comparisons appear to us to be impossible at the present time, however, due to uncertainties in the magnitudes of the zero T penetration depths.

In the case of thermal conductivity, only the coefficient of the linear T term is relevant since it can be unambiguously assigned to electronic transport. We find again in the two promising cases that qualitative thermal conductivity anisotropy in agreement with experiment is found. For this calculation, semiquantitative agreement with experiment can be obtained once the disorder scattering rate and overall Fermi velocity renormalization is fixed. One further remarkable aspect of the experiments explained by the 3D Fermi surface and order parameter models we have considered is that the linear-T ab-plane thermal conductivity is substantially smaller than one might expect on the basis of simple dimensional analysis, reflecting the small phase space from the short nodal segments near the top of the Brillouin zone. The c-axis measurements of Reid et al.[21], in this picture, force one to the conclusion that κ_{ab} is not zero in these materials, as previously reported, but must be so small as to be unresolvable within current experiments.

Further conclusions can be drawn from study of the magnetic field dependence of the residual linear terms within the semiclassical approach. The observed field dependence in the 122 is quite similar to nodal systems in clean limit, including the size of the term. This suggests that the small nodal structures probed by the c-axis transport are not giving rise to the field dependence; instead, this contribution is dominated by the remaining Fermi surface sheets which have no nodes but rather deep gap minima which run the length of the Fermi cylinder[18]. An immediate consequence is that in the cases which appear promising relative to experiment in zero field, the ab-plane transport is immediately enhanced upon application of a small field, leading to comparable nodal-type field variation of the thermal conductivity in both directions, as reported in Ref. 21.

Finally, we have briefly discussed how the nodal structures which appear to us to be the most likely in this 3D system could be detected. We propose a full angle-dependent measurement of the directional thermal conductivity. Weak 4-fold oscillations of the specific heat have been reported in other Fe-based superconductors[67], and discussed theoretically recently.[72] On the other hand, if the heat current is along c and the field is always in the plane, the unique features of the nodal structures near the top of the Brillouin zone face will be missed. Therefore measurements at polar angles of the magnetic field between 0 and 90 degrees with respect to the plane may be useful. Our study has found, however, that the angular dependence of this signal is probably dominated

by the structures on electron, not hole sheets; therefore these small hole pocket signatures may be difficult to observe.

Our calculations provide further evidence for the conjecture of an "intrinsic sensitivity" of the gap structures in the Fe-based superconductors to small perturbations in electronic structure[14]. Recall that according to Graser *et al.*[26], the nodes which appear near the top of the Brillouin zone on the hole pockets in these systems are probably related to the suppression of d_{xz}/d_{yz} orbital weight there, which in turn occurs because of special features in the 122 crystal structure not shared by other Fe-pnictides.

Within our model, the increase of normalized thermal conductivity anisotropy observed by Reid *et al.*[21] in Co-doped Ba-122 may be attributed to the increased flaring of the Fermi surface sheet as seen in ARPES experiments and DFT calculations. This is a nontrivial effect due not to the increase of the average c-axis Fermi velocity but the increase of this component at the position of the gap nodes. There are clearly other effects present, however, including the possible occurrence of nodes on the electron sheets for the most overdoped systems, as indicated by the non-zero κ_{ab}. It is an important challenge to construct a microscopic theory which can simultaneously describe the evolution of the Fermi surface and gap structure with doping.

Acknowledgments

[1] K. Ishida, Y. Nakai, and H. Hosono, J. Phys. Soc. Jpn. **78**, 062001 (2009).

[2] D. C. Johnston, Advances in Physics **59**, 803 (2010).

[3] L. Boeri, O. V. Dolgov, and A. A. Golubov, Phys. Rev. Lett. **101**, 026403 (2008).

[4] L. Boeri, M. Calandra, I. I. Mazin, O. V. Dolgov, and F. Mauri, Phys. Rev. B **82**, 020506 (2010).

[5] L. Stojchevska, P. Kusar, T. Mertelj, V. V. Kabanov, X. Lin, G. H. Cao, Z. A. Xu, and D. Mihailovic, Phys. Rev. B **82**, 012505 (2010).

[6] I. I. Mazin, D. J. Singh, M. D. Johannes, and M. H. Du, Phys. Rev. Lett. **101**, 057003 (2008).

[7] S. Graser, T. A. Maier, P. J. Hirschfeld, and D. J. Scalapino, New. J. Phys. **11** (2009).

[8] A. V. Chubukov, D. V. Efremov, and I. Eremin, Phys. Rev. B **78**, 134512 (2008).

[9] A. V. Chubukov, M. G. Vavilov, and A. B. Vorontsov, Phys. Rev. B **80**, 140515 (2009).

[10] K. Kuroki, S. Onari, R. Arita, H. Usui, Y. Tanaka, H. Kontani, and H. Aoki, Phys. Rev. Lett. **101**, 087004 (2008).

[11] F. Wang, H. Zhai, Y. Ran, A. Vishwanath, and D. H. Lee, Phys. Rev. Lett. **102**, 047005 (2009).

[12] F. Wang, H. Zhai, and D. H. Lee, Phys. Rev. B **81**, 184512 (2010).

[13] R. Thomale, C. Platt, J. Hu, C. Honerkamp, and B. A. Bernevig, Phys. Rev. B **80**, 180505 (2009).

[14] A. F. Kemper, T. A. Maier, S. Graser, H.-P. Cheng, P. J. Hirschfeld, and D. J. Scalapino, New. J. Phys. **12**, 073030 (2010).

[15] X. G. Luo, M. A. Tanatar, J.-P. Reid, H. Shakeripour, N. Doiron-Leyraud, N. Ni, S. L. Budko, P. C. Canfield, H. Luo, Z. Wang, et al., Phys. Rev. B **80**, 140503(R) (2009).

[16] L. Ding, J. K. Dong, S. Y. Zhou, T. Y. Guan, X. Qiu, C. Zhang, L. J. Li, X. Lin, G. H. Cao, Z. A. Xu, et al., New. J. Phys. **11**, 093018 (2009).

[17] M. A. Tanatar, J.P. Reid, H. Shakeripour, X. G. Luo, N. Doiron-Leyraud, N. Ni, S. L. Bud'ko, P. C. Canfield, R. Prozorov, and L. Taillefer, Phys. Rev. Lett. **104**, 067002

(2010).

[18] V. Mishra, G. Boyd, S. Graser, T. Maier, P. J. Hirschfeld, and D. J. Scalapino, Phys. Rev. B **79**, 094512 (2009).

[19] Y. Bang, Phys. Rev. Lett. **104**, 217001 (2010).

[20] C. Martin, H. Kim, R. T. Gordon, N. Ni, V. G. Kogan, S. L. Bud'ko, P. C. Canfield, M. A. Tanatar, and R. Prozorov, Phys. Rev. B **81**, 060505 (2010).

[21] J.-P. Reid, M. A. Tanatar, X. G. Luo, H. Shakeripour, N. Doiron-Leyraud, N. Ni, S. L. Bud'ko, P. C. Canfield, R. Prozorov, and L. Taillefer, Phys. Rev. B **82**, 064501 (2010).

[22] L. Taillefer, B. Lussier, R. Gagnon, K. Behnia, and H. Aubin, Phys. Rev. Lett. **79**, 483 (1997).

[23] I. Kosztin and A. J. Leggett, Phys. Rev. Lett. **79**, 135 (1997).

[24] P. Hirschfeld, D. Vollhardt, and P. Wolfle, Solid State Commun. **59**, 111 (1986).

[25] F. Wang, H. Zhai, Y. Ran, A. Vishwanath, and D.-H. Lee, Phys. Rev. Lett. **102**, 047005 (2009).

[26] S. Graser, A. F. Kemper, T. A. Maier, H.-P. Cheng, P. J. Hirschfeld, and D. J. Scalapino, Phys. Rev. B **81**, 214503 (2010).

[27] K. Suzuki, H. Usui, and K. Kuroki, J. Phys. Soc. Jpn. **80**, 013710 (2011).

[28] C. Martin, M. E. Tillman, H. Kim, M. A. Tanatar, S. K. Kim, A. Kreyssig, R. T. Gordon, M. D. Vannette, S. Nandi, V. G. Kogan, et al., Phys. Rev. Lett. **102**, 247002 (2009).

[29] D. J. Singh, Phys. Rev. B **78**, 094511 (2008).

[30] A. S. Sefat, R. Jin, M. A. McGuire, B. C. Sales, D. J. Singh, and D. Mandrus, Phys. Rev. Lett. **101**, 117004 (2008).

[31] G.T. Wang, Y. Qian, G. Xu, X. Dai, and Z. Fang, Phys. Rev. Lett. **104**, 047002 (2010).

[32] W. Malaeb, T. Yoshida, A. Fujimori, M. Kubota, K. Ono, K. Kihou, P. M. Shirage, H. Kito, A. Iyo, H. Eisaki, et al., J. Phys. Soc. Jpn. **78**, 123706 (2009).

[33] J. Fink, S. Thirupathaiah, R. Ovsyannikov, H. A. Dürr, R. Follath, Y. Huang, S. de Jong, M. S. Golden, Y.-Z. Zhang, H. O. Jeschke, et al., Phys. Rev. B **79**, 155118 (2009).

[34] S. Thirupathaiah, S. de Jong, R. Ovsyannikov, H. A. Dürr, A. Varykhalov, R. Follath, Y. Huang, R. Huisman, M. S. Golden, Y.-Z. Zhang, et al., Phys. Rev. B **81**, 104512 (2010).

[35] T. Kondo, R. M. Fernandes, R. Khasanov, C. Liu, A. D. Palczewski, N. Ni, M. Shi, A. Bostwick, E. Rotenberg, J. Schmalian, et al., Phys. Rev. B **81**, 060507 (2010).

[36] V. Brouet, M. Marsi, B. Mansart, A. Nicolaou, A. Taleb-Ibrahimi, P. Le Fèvre, F. Bertran, F. Rullier-Albenque, A. Forget, and D. Colson, Phys. Rev. B **80**, 165115 (2009).

[37] L. Ortenzi, E. Cappelluti, L. Benfatto, and L. Pietronero, Phys. Rev. Lett. **103**, 046404 (2009).

[38] A. F. Kemper, C. Cao, P. J. Hirschfeld, and H.-P. Cheng, Phys. Rev. B **80**, 104511 (2009).

[39] V. Mishra, A. Vorontsov, P. J. Hirschfeld, and I. Vekhter, Phys. Rev. B **80**, 224525 (2009).

[40] L.S. Borkowski and P.J. Hirschfeld, Phys. Rev. B **49**, 15404 (1994).

[41] D. E. Sheehy, T. P. Davis, and M. Franz, Phys. Rev. B **70**, 054510 (2004).

[42] T. J. Williams, A. A. Aczel, E. Baggio-Saitovitch, S. L. Bud'ko, P. C. Canfield, J. P. Carlo, T. Goko, J. Munevar, N. Ni, Y. J. Uemura, et al., Phys. Rev. B **80**, 094501 (2009).

[43] R. T. Gordon, N. Ni, C. Martin, M. A. Tanatar, M. D. Vannette, H. Kim, G. D. Samolyuk, J. Schmalian, S. Nandi, A. Kreyssig, et al., Phys. Rev. Lett. **102**, 127004 (2009).

[44] R. T. Gordon, H. Kim, N. Salovich, R. W. Giannetta, R. M. Fernandes, V. G. Kogan, T. Prozorov, S. L. Bud'ko, P. C. Canfield, M. A. Tanatar, et al., Phys. Rev. B **82**, 054507 (2010).

[45] L. Luan, O. M. Auslaender, T. M. Lippman, C. W. Hicks, B. Kalisky, J.-H. Chu, J. G. Analytis, I. R. Fisher, J. R. Kirtley, and K. A. Moler, Phys. Rev. B **81**, 100501 (2010).

[46] L. Luan, O. M. Auslaender, T. M. Lippman, C. W. Hicks, B. Kalisky, J.-H. Chu, J. G. Analytis, I. R. Fisher, J. R. Kirtley, and K. A. Moler, Phys. Rev. B **81**, 100501 (2010).

[47] M. Nakajima, S. Ishida, K. Kihou, Y. Tomioka, T. Ito, Y. Yoshida, C. H. Lee, H. Kito, A. Iyo, H. Eisaki, et al., Phys. Rev. B **81**, 104528 (2010).

[48] R. Prozorov and R. W. Giannetta, Superconductor Science and Technology **19**, R41 (2006).

[49] D. Einzel, P. J. Hirschfeld, F. Gross, B. S. Chandrasekhar, K. Andres, H. R. Ott, J. Beuers, Z. Fisk, and J. L. Smith, Phys. Rev. Lett. **56**, 2513 (1986).

[50] A. B. Vorontsov, M. G. Vavilov, and A. V. Chubukov, Phys. Rev. B **79**, 140507 (2009).

[51] M. A. Tanatar, N. Ni, C. Martin, R. T. Gordon, H. Kim, V. G. Kogan, G. D. Samolyuk, S. L. Bud'ko, P. C. Canfield, and R. Prozorov, Phys. Rev. B **79**, 094507 (2009).

[52] R. Prozorov, M. A. Tanatar, R. T. Gordon, C. Martin, H. Kim, V. G. Kogan, N. Ni, M. E. Tillman, S. L. Bud'Ko, and P. C. Canfield, Physica C **469**, 582 (2009).

[53] V. Ambegaokar and A. Griffin, Phys. Rev. **137**, A1151 (1965).

[54] P. J. Hirschfeld, P. Wölfle, and D. Einzel, Phys. Rev. B **37**, 83 (1988).

[55] A. C. Durst and P. A. Lee, Phys. Rev. B **62**, 1270 (2000).

[56] M. Yamashita, N. Nakata, Y. Senshu, S. Tonegawa, K. Ikada, K. Hashimoto, H. Sugawara, T. Shibauchi, and Y. Matsuda, Phys. Rev. B **80**, 220509 (2009).

[57] K. Hashimoto, M. Yamashita, S. Kasahara, Y. Senshu, N. Nakata, S. Tonegawa, K. Ikada, A. Serafin, A. Carrington, T. Terashima, et al., Phys. Rev. B **81**, 220501 (2010).

[58] C. Kübert and P. J. Hirschfeld, Phys. Rev. Lett. **80**, 4963 (1998).

[59] K. Kuroki, H. Usui, S. Onari, R. Arita, and H. Aoki, Phys. Rev. B **79**, 224511 (2009).

[60] G. E. Volovik, JETP Lett. **58**, 469 (1993).

[61] I. Vekhter, P. J. Hirschfeld, J. P. Carbotte, and E. J. Nicol, Phys. Rev. B **59**, R9023 (1999).

[62] I. Vekhter, P. J. Hirschfeld, and E. J. Nicol, Phys. Rev. B **64**, 064513 (2001).

[63] M. Franz and Z. Tesanovic, Phys. Rev. Lett. **84**, 554 (2000).

[64] D. Knapp, C. Kallin, and A. J. Berlinsky, Phys. Rev. B **64**, 014502 (2001).

[65] Y. Matsuda, K. Izawa, and I. Vekhter, Journal of Physics Condensed Matter **18**, 705 (2006).

[66] S. Graser, G. R. Boyd, C. Cao, H.-P. Cheng, P. J. Hirschfeld, and D. J. Scalapino, Phys. Rev. B **77**, 180514 (2008).

[67] B. Zeng, G. Mu, H. Q. Luo, T. Xiang, H. Yang, L. Shan, C. Ren, I. I. Mazin, P. C. Dai, and H. Wen, Nat. Comm. **1**, 112 (2010).

[68] A. Vorontsov and I. Vekhter, Phys. Rev. Lett. **96**, 237001 (2006).

[69] A. B. Vorontsov and I. Vekhter, Phys. Rev. B **75**, 224501 (2007).

[70] G. R. Boyd, P. J. Hirschfeld, I. Vekhter, and A. B. Vorontsov, Phys. Rev. B **79**, 064525 (2009).

[71] H. Kim, R. T. Gordon, M. A. Tanatar, J. Hua, U. Welp, W. K. Kwok, N. Ni, S. L. Bud'ko, P. C. Canfield, A. B. Vorontsov, et al., Phys. Rev. B **82**, 060518 (2010).

[72] A. B. Vorontsov and I. Vekhter, Phys. Rev. Lett. **105**, 187004 (2010).